

Can Understanding and Generation Truly Benefit Together — or Just Coexist?

Zhiyuan Yan^{1,2*}, Kaiqing Lin^{1*}, Zongjian Li^{1,3*}, Junyan Ye^{4*}, Hui Han¹, Zhendong Wang⁵, Hao Liu², Bin Lin^{1,3}, Hao Li¹, Xue Xu², Xinyan Xiao^{2†}, Jingdong Wang², Haifeng Wang², Li Yuan^{1†}

* Equal Contributors, † Corresponding Authors

¹PKU, ²Baidu ERNIE, ³Rabbitpre AI, ⁴SYSU, ⁵USTC

{zhiyuanyan@stu., yuanli-ece@}pku.edu.cn

<https://github.com/PKU-YuanGroup/UAE>

Abstract

The pursuit of unified multimodal models (UMMs) has long been hindered by a fundamental schism between understanding and generation. Current approaches typically treat them as separate endeavors with disjoint objectives, leading to missing cross-task mutual benefits. We argue that true unification requires more than just merging two tasks; it requires a unified, foundational objective that intrinsically links them. In this paper, we introduce an insightful paradigm through the **Auto-Encoder lens**—understanding as the encoder (I2T) that compresses images into text, and generation as the decoder (T2I) that reconstructs images from that text. Using reconstruction fidelity as the unified training objective, we enforce the coherent bidirectional information flow between the understanding (encoding) and generation (decoding) processes, bringing mutual gains. To implement this, we propose **UAE**, a novel framework for unified multimodal learning. We begin by pre-training the decoder with large-scale long-context image captions to capture fine-grained semantic and complex spatial relationships. We then propose **Unified-GRPO** via reinforcement learning (RL), which covers three stages: (1) A cold-start phase to gently initialize both encoder and decoder with a semantic reconstruction loss; (2) *Generation for Understanding*, where the encoder is trained to generate informative captions that maximize the decoder’s reconstruction quality, enhancing its visual understanding; (3) *Understanding for Generation*, where the decoder is refined to reconstruct from these captions, forcing it to leverage every detail and improving its long-context instruction following and generation fidelity. For evaluation, we introduce **Unified-Bench**, the first benchmark tailored to assess the degree of unification of the UMMs. A surprising *“aha moment”* arises within the multimodal learning domain: as RL progresses, the encoder autonomously produces more descriptive captions, while the decoder simultaneously demonstrates a profound ability to understand these intricate descriptions, resulting in reconstructions of striking fidelity. This co-evolution provides compelling evidence of a breakthrough toward genuine multimodal unification and intelligence.

1 Introduction

Unifying multimodal models (UMMs) that support both generation and understanding remains an urgent, unresolved challenge [33, 5, 35, 39, 25, 14, 45, 41, 9, 11]. But many key questions still exist: How should gains in understanding translate into better generation—and vice versa? Should both be trained under a joint objective rather than separate losses? And if that, how can that objective be optimized in a complementary, mutually reinforcing way—an area still underexplored?

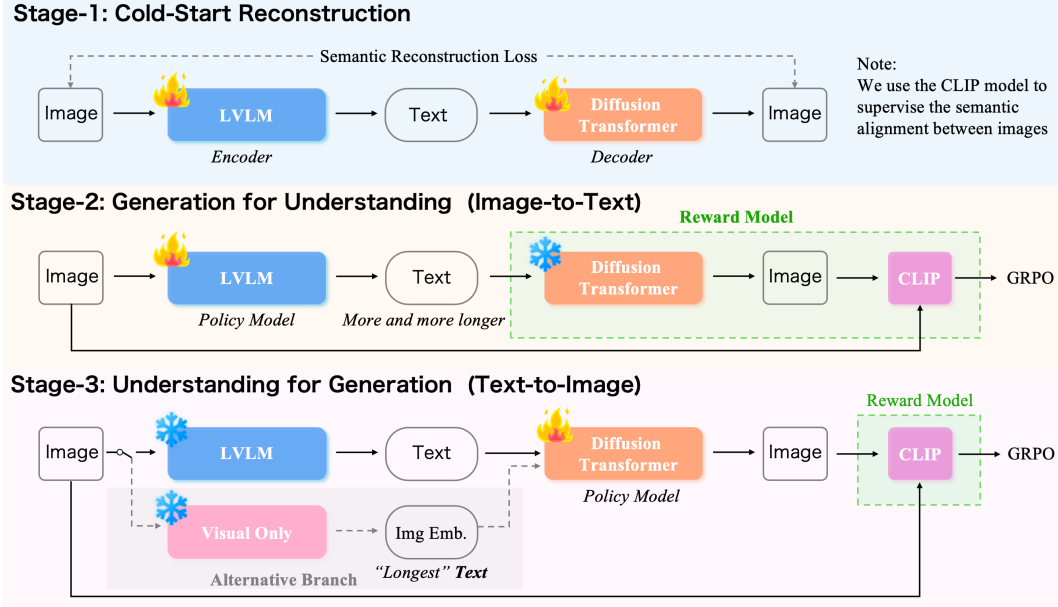


Figure 2: The overall workflow of our Unified-GRPO, consisting of three stages: cold-start reconstruction, generation for understanding, and understanding for generation.

Cold-start reconstruction phase to gently initialize both the encoder and decoder. **(2) Generation for Understanding**—the encoder is trained to produce informative captions that maximize the decoder’s reconstruction quality, thereby strengthening visual understanding; **(3) Understanding for Generation**—the decoder is refined to reconstruct from the text, forcing it to leverage every detail and improving long-context instruction following and generation fidelity. We further explore using the image embedding from the visual encoder instead of the output caption from the understanding model, as we believe the image embedding can be viewed as the most informative “text”. We fine-tune the decoder in a progressive manner, from the shorter caption to the longer caption, and even the “longest caption” (targeted image) for generation.

Surprisingly, **we observe an emergent “aha moment” in multimodal learning**: as RL progresses, the encoder autonomously generates longer, richer captions, while the decoder concurrently improves its ability to interpret them, yielding reconstructions of striking fidelity, as demonstrated in Fig. 1. This co-evolution offers compelling evidence of progress toward genuine multimodal unification.

In summary, our work makes the following key contributions:

- We propose **UAE, the first work based on an Auto-Encoder unification principle**, casting understanding as the encoder (I2T) and generation as the decoder (T2I), with reconstruction as a measurable signal of cross-modal information coherence. This resolves the long-standing schism between understanding and generation and provides an actionable, verifiable objective for unified multimodal models (UMMs).
- We develop **Unified-GRPO, the first reinforcement learning (RL) scheme that jointly and mutually improves both understanding and generation**: (1) *Generation for Understanding* trains the encoder to produce informative captions that maximize reconstruction quality; (2) *Understanding for Generation* refines the decoder to reconstruct from these captions, forcing it to leverage every detail. This bidirectional optimization forms a positive feedback loop toward genuine unification.
- We report an emergent **“aha moment” in multimodal learning**: as RL progresses, the encoder autonomously emits longer, more descriptive captions while the decoder simultaneously achieves strikingly faithful reconstructions. This co-evolution offers compelling empirical evidence for unified multimodal intelligence.
- We release **Unified-Bench**, to the best of our knowledge, the first benchmark explicitly designed to **measure the degree of unification** in UMMs, rather than individually evaluating the generation or understanding capabilities.

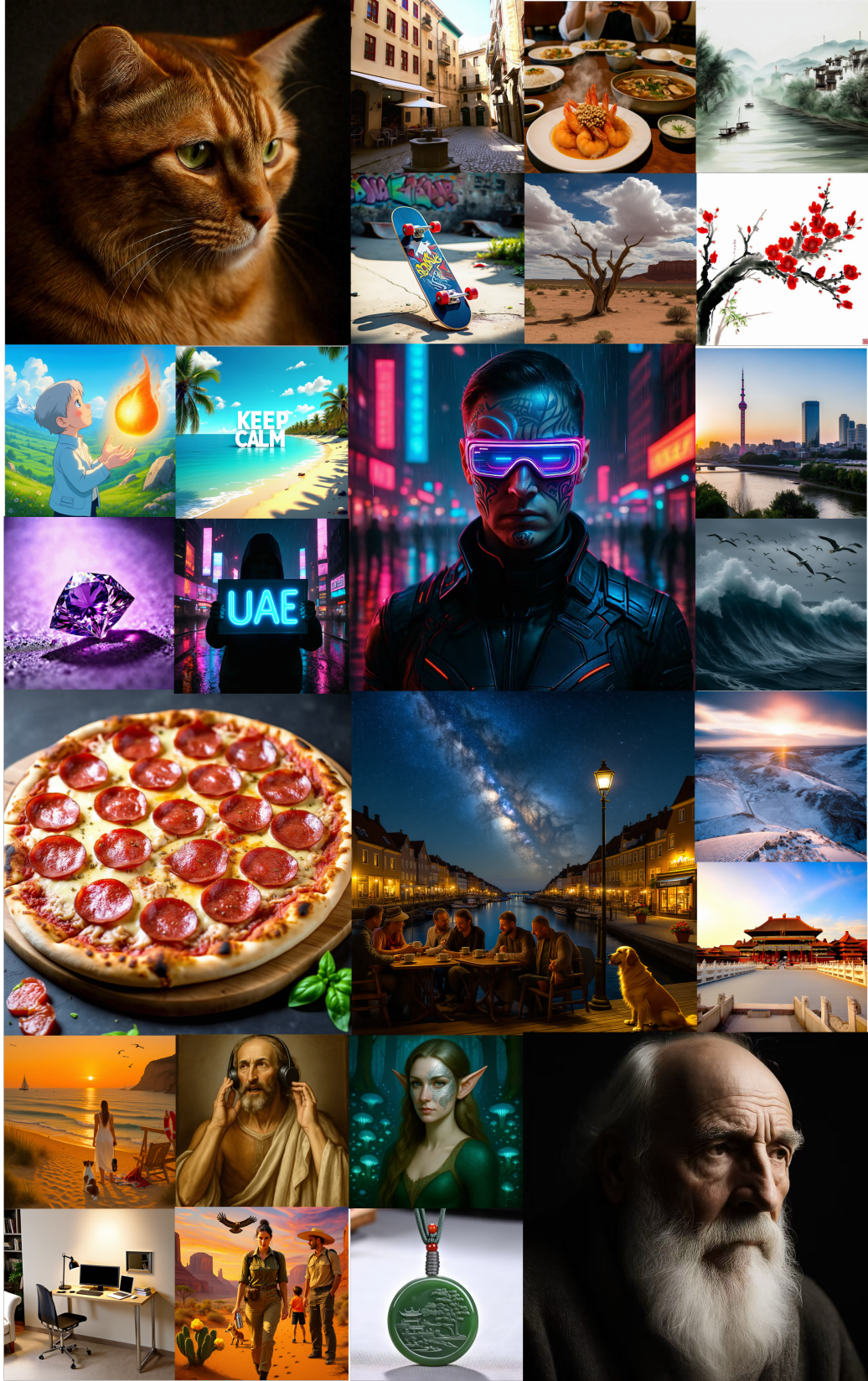


Figure 3: Visualization results of UAE at 1024×1024 resolution.

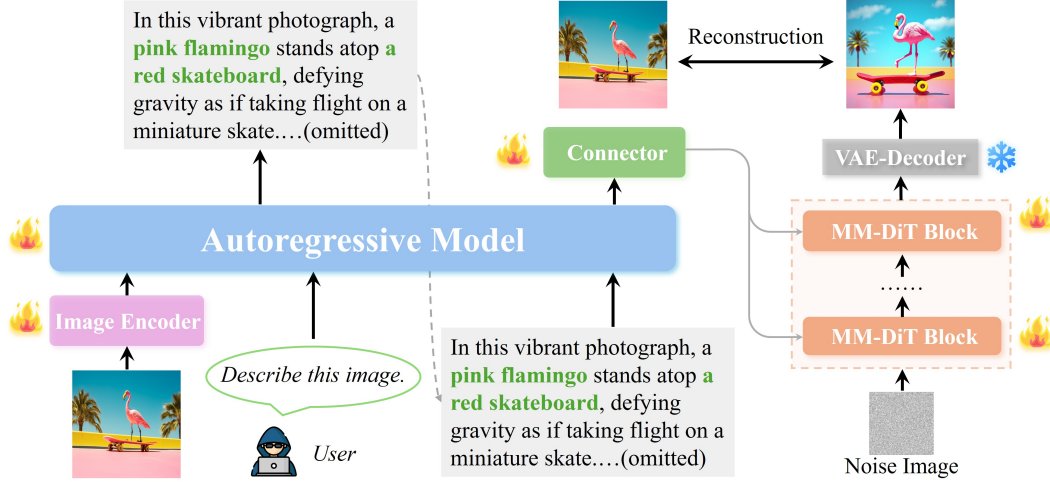


Figure 4: The detailed illustration of our framework design. Our framework employs an autoregressive LVLM to process the input image embedding derived from the original image. The model generates a text caption, which is then fed into the autoregressive LLM. From this, we extract the final hidden state and project it through a connector into the decoder’s feature space, where it serves as the condition for image generation.

2 UAE Methodology

2.1 Architecture

Overview. Our system follows a compact *encode–project–decode AE-based* design that couples a Large Vision–Language Model (LVLM) for multimodal understanding with a strong diffusion transformer for image synthesis, as illustrated in Fig. 4. The LVLM converts the input (image and optional prompt) into a rich semantic representation; a lightweight projector then maps this representation to the decoder’s conditioning space; finally, the diffusion model expands this condition into pixels. This separation keeps the interface minimal, preserves the strengths of each component, and makes the system modular and scalable.

Encoder. We adopt **Qwen-2.5-VL 3B** [3] as the base LVLM encoder. It consists of a visual encoder paired with an autoregressive language model capable of processing vision–language inputs. For generation, the LVLM autoregressively processes the prompt and multimodal context to produce a high-dimensional, context-rich representation. Rather than passing raw text to the decoder, we extract the *last hidden state* from the LLM and feed it to a small MLP projector. The projected embedding serves as the decoder’s conditioning signal, providing a compact semantic summary grounded in the LVLM’s learned world knowledge.

Decoder. For the visual decoder, we use a well-pretrained diffusion model to reconstruct image pixels from the LVLM’s semantic representation. Concretely, we employ **SD3.5-large** [10] and add a minimal projector head (two linear layers) to match the LVLM embedding dimension to the conditioning channels expected by SD3.5. During synthesis, the diffusion decoder takes the projected semantic condition as input and generates images in the pixel space. This setup leverages the LVLM for high-level semantics while relying on the diffusion backbone for photorealistic, high-fidelity rendering.

LoRA-Adaptation. Following previous works [21, 40], we apply LoRA [15] adaptation for both the encoder and decoder for RL post-training, as it can help preserve the rich semantic knowledge learned from pre-training while efficiently learning novel knowledge from the new task. We maintain the same settings of LoRA with Flow-GRPO [21].

2.2 Data

SFT (long-context T2I). We construct a 700K text–image corpus to warm up the decoder for long-context generation. Each sample pairs a 1024-resolution image with a detailed caption above 250 English words. Captions are produced by InternVL-78B [6] over our private image collection, emphasizing objects, attributes, spatial relations, and scene composition. We show two examples of our proposed dataset (see Fig. 8 and Fig. 9). During pretraining, the caption is used as the input prompt and the diffusion transformer is trained to synthesize the corresponding image from this text.

GPT-4o distillation (50K). To further strengthen caption quality and stylistic consistency, we use the auto-script from GPT-ImgEval [41] to distill an additional 50K high-resolution samples from *GPT-4o*, yielding high-fidelity, long-form (around 300 words) descriptions. These distilled pairs are included in the pretraining mix to anchor dense semantics and improve instruction following.

RL stage data (1K). For the reinforcement learning phase, we carefully curate 1K high-quality real-photography images and supplement them with a subset of Echo-4o data [42]. These images serve as targets for reconstruction-driven optimization, where the model is encouraged to close the loop—caption then reconstruct—so that improvements in understanding (captioning) translate into more faithful generation.

2.3 Unified-GRPO

Pipeline of Image Reconstruction. In our method, Large Vision-Language Model (LVLM; e.g., Qwen-2.5-VL [3]) as an *autoregressive* encoder for understanding, and Diffusion Transformer (DiT; e.g., SD-3.5-large [10]) as a decoder for generation. Given a image x , the LVLM autoregressively produces a collection of tokens $y_{1:T}$ with hidden states $\{h_t\}_{t=1}^T$. Subsequently, we take the *last* hidden state h_T and map it through an MLP projector $g(\cdot)$ to obtain the condition vector $c_{\text{text}} = g(h_T) \in \mathbb{R}^d$. As an alternative branch, we use a *visual-only* condition $c_{\text{img}} = g(v)$, where $v = f_{\text{vis}}(x)$ is the image embedding from the LVLM’s vision encoder (or a dedicated image encoder). The decoder is an SD3-style diffusion transformer (DiT); it generates $\tilde{x} \sim p_{\theta}(\cdot | c)$ with $c \in \{c_{\text{text}}, c_{\text{img}}\}$. Finally,

Algorithm of Group Relative Policy Optimization (GRPO). We adopt the GRPO algorithm [30] to alternately optimize the understanding (*i.e.*, Encoder) and generation (*i.e.*, Decoder) of UAE, aiming to leverage the synergistic benefits between understanding and generation. In GRPO, for a given input, a policy model π generates a set of G trajectories, denoted $\{o_i\}_{i=1}^G$. In our application, each trajectory o_i corresponds to the generation process of a single reconstructed image \tilde{x}_i , resulting in a group of images $\{\tilde{x}_i\}_{i=1}^G$. For this task, the reward signal is provided by a **reconstruction reward**, which we define using a frozen CLIP image encoder $f_I(\cdot)$ as:

$$R_i(x, \tilde{x}_i) = \cos \langle f_I(x), f_I(\tilde{x}_i) \rangle.$$

The estimation of an advantage \tilde{A}_i for each trajectory are shown following:

$$\tilde{A}_i = \frac{R_i - \text{mean}(\{R_k\}_{k=1}^G)}{\text{std}(\{R_k\}_{k=1}^G)}. \quad (1)$$

The policy’s parameters θ are then updated by maximizing the GRPO objective function:

$$\mathcal{J}(\theta) = \mathbb{E}_{c \sim \mathcal{C}, \{o_i\}_{i=1}^G \sim \pi_{\theta_{\text{old}}}(\cdot | c)} \left[\frac{1}{G} \sum_{i=1}^G \frac{1}{T_i} \sum_{t=0}^{T_i-1} \left(\min(r_t^i(\theta) \tilde{A}_i, \text{clip}(r_t^i(\theta), 1 - \varepsilon, 1 + \varepsilon) \tilde{A}_i) - \beta \mathbb{D}_{\text{KL}}(\pi_{\theta} \| \pi_{\theta_{\text{ref}}}) \right) \right], \quad (2)$$

where $r_t^i(\theta)$ is the probability ratio between the current and old policies, and T_i is the length of i -th trajectory. In Stage-2 and 3, we introduce the specific instantiations of the policy and the trajectory.

Stage-1: Cold-start reconstruction. To ensure the basic alignment, we *jointly* initialize the LVLM and the DiT *only* with a semantic reconstruction loss that closes the image→LVLM→DiT loop. For each x , form a condition c (c_{text}), generate $\tilde{x} \sim p_{\theta}(\cdot | c)$, and minimize

$$\mathcal{L}_{\text{Stage1}}(\phi, \theta) = \mathbb{E}_{x \sim \mathcal{D}} [1 - \cos \langle f_I(x), f_I(\tilde{x}_i) \rangle]. \quad (3)$$

Method	CLIP [28]	LongCLIP [44]	DINO-v2 [24]	DINO-v3 [31]	Overall
GPT-4o-Image [23]	<u>90.42</u>	94.37	<u>81.74</u>	<u>77.27</u>	<u>85.95</u>
BAGEL [8]	88.97	93.35	78.55	73.05	83.48
BLIP-3o [4]	84.84	90.24	68.31	62.86	76.56
Janus-Pro [5]	88.72	93.45	78.30	70.61	82.77
OmniGen2 [36]	88.36	93.11	77.70	74.07	83.31
Show-o [38]	80.18	86.75	58.20	51.51	69.16
UniWorld-V1 [20]	85.49	91.53	72.12	66.83	78.99
UAE	90.50	<u>94.35</u>	81.98	77.54	86.09

Table 1: Comparisons of unified score on **Unified-Bench**, the first benchmark specifically for evaluating the unification between understanding and generation models in the unified multimodal systems. **Bold** indicates the best result, and underlined denotes the second best.

Here, there is neither an autoregressive loss for the LVLM (the I2T loss) nor a denoising loss for the DiT (the T2I loss). This stage can ensure an effective collaboration between LVLM and DiT for image reconstruction.

Stage-2: Generation for Understanding. In this stage, the LVLM π_ϕ serves as the policy, while the DiT p_θ is *frozen* and functions as part of the reward evaluation environment alongside the CLIP encoder. For each input image x , we sample a group of G caption sequences $\{y^{(i)}\}_{i=1}^G$ from the old policy $\pi_{\phi_{\text{old}}}(\cdot | x)$. From each sequence $y^{(i)}$, we extract the last hidden state $h_T^{(i)}$ to form a condition $c^{(i)} = g(h_T^{(i)})$, which is subsequently used to synthesize an image $\tilde{x}^{(i)} \sim p_\theta(\cdot | c^{(i)})$. The LVLM’s parameters ϕ are then updated by maximizing the GRPO objective in Equation (2). In this context, each trajectory o_i corresponds to a sampled caption sequence $y^{(i)} = (y_1^{(i)}, \dots, y_{T(i)}^{(i)})$. The probability ratio is thus defined as $r_t^i(\phi) = \frac{\pi_\phi(y_t^{(i)} | x, y_{<t}^{(i)})}{\pi_{\phi_{\text{old}}}(y_t^{(i)} | x, y_{<t}^{(i)})}$. This stage trains the LVLM to emit last-hidden representations that *maximize* the decoder’s reconstruction quality.

Stage-3: Understanding for Generation. The roles are now reversed: the image generation model p_θ (e.g., DiT) acts as *policy*, while the LVLM is *frozen*, serving to provide conditions $c = \{c_{\text{text}}, c_{\text{img}}\}$ for generation. Note that c_{img} is an alternative option, as we find that it produces very similar results to those using only the LVLM output caption. We argue that the semantic similarity between the ultra-descriptive caption and original image embedding can be high, resulting in a similar condition for decoder for generation (see Sec. 5 for detailed discussion). We optimize p_θ using the GRPO by sampling reverse-time generation trajectories. For a given condition c , the policy p_θ generates a group of G images $\{x_0^i\}_{i=1}^G$. In this context, each trajectory o_i corresponds to a full reverse-time sequence $(x_T^i, x_{T-1}^i, \dots, x_0^i)$, representing the denoising process from an initial noise sample x_T^i to the final image x_0^i . The parameters θ of the generation model are then updated by maximizing the GRPO objective in Equation (2). For this stage, the per-step likelihood ratio is given by:

$$r_t^i(\theta) = \frac{p_\theta(x_{T-1}^i | x_T^i, c)}{p_{\theta_{\text{old}}}(x_{T-1}^i | x_T^i, c)}. \quad (4)$$

The stochasticity arises from the SDE sampling of the reverse process.

3 Unified-Bench: A Benchmark tailored for Evaluating the Unified Models

Motivation. As illustrated in Fig. 1, we view *understanding* (I→T) and *generation* (T→I) as a closed loop whose two halves should *mutually enhance* each other. Judging image realism alone or caption fidelity alone cannot reveal whether a system is truly *unified*. We therefore adopt a reconstruction-based similarity—our **unified-score**—to directly test whether the semantics distilled during understanding are sufficient for faithful regeneration, and whether regeneration in turn validates the completeness of the understanding.

Unified-Bench protocol. We construct **Unified-Bench** to measure this mutuality: starting from 100 diverse source images, the model first produces a detailed caption using the prompt, “You are

Method	Single object	Two object	Counting	Colors	Position	Color attribution	Overall
Dedicated T2I							
SDv2.1 [29]	0.98	0.5	0.44	0.85	0.07	0.17	0.50
SDXL [26]	0.98	0.74	0.39	0.85	0.15	0.23	0.55
IF-XL [7]	0.97	0.74	0.66	0.81	0.13	0.35	0.61
Lumina-Next [46]	0.92	0.46	0.48	0.70	0.09	0.13	0.46
SD3-medium [1]	0.99	0.94	0.72	0.89	0.33	0.60	0.74
SD3.5-large [10]	0.98	0.89	0.73	0.83	0.34	0.47	0.71
FLUX.1-dev [18]	0.99	0.81	0.79	0.74	0.20	0.47	0.67
NOVA [9]	0.99	0.91	0.62	0.85	0.33	0.56	0.71
OmniGen [37]	0.98	0.84	0.66	0.74	0.40	0.43	0.68
Unified Model							
TokenFlow-XL [27]	0.95	0.60	0.41	0.81	0.16	0.24	0.55
Janus [35]	0.97	0.68	0.30	0.84	0.46	0.42	0.61
Janus Pro [5]	0.99	0.89	0.59	<u>0.90</u>	0.79	0.66	0.80
Emu3-Gen [33]	0.98	0.71	0.34	0.81	0.17	0.21	0.54
Show-o [38]	0.98	0.80	0.66	0.84	0.31	0.50	0.68
MetaQuery-XL [†] [25]	-	-	-	-	-	-	0.80
BLIP3-o 8B [4]	-	-	-	-	-	-	0.84
UniWorld-V1 [20]	0.99	0.93	0.79	0.89	0.49	0.70	0.80
UniWorld-V1 [†] [20]	0.98	0.93	0.81	0.89	0.74	0.71	0.84
OmniGen2 [36]	1	<u>0.95</u>	0.64	0.88	0.55	0.76	0.80
BAGEL [8]	0.99	0.94	0.81	0.88	0.64	0.63	0.82
BAGEL [†] [8]	0.98	<u>0.95</u>	0.84	0.95	<u>0.78</u>	0.77	<u>0.88</u>
UAE	1	0.89	0.84	<u>0.90</u>	0.71	0.79	0.86
UAE[†]	1	0.97	<u>0.82</u>	0.95	0.73	0.84	0.89

Table 2: Comparisons of text-to-image generation capability on GenEval [13] benchmark. ‘†’ refers to the methods using LLM rewriter. **Bold** indicates the best result, and underlined denotes the second best.

a helpful assistant. Your task is to provide an accurate description based on the content of the image, helping the generation model to create an image based on your description. Ensure that your description is clear and comprehensive, so that the generation model can produce an image that closely matches the content of the image based on your input.” The same model then synthesizes an image from its *own* caption. We compute unified-scores between the reconstruction and the source using four widely adopted vision backbones—CLIP, LongCLIP, DINO-v2, and DINO-v3—and report per-backbone similarities and an overall summary.

4 Results

4.1 Unified Evaluation

We assess the unified degree with the proposed Unified-Bench. Tab. 1 shows that our **UAE** achieves the best **Overall** unified score (86.09), surpassing GPT-4o-Image (85.95). Specifically, UAE obtains the top results on CLIP (90.50), DINO-v2 (81.98), and DINO-v3 (77.54), and statistical parity on LongCLIP (94.35 vs. 94.37). These consistent gains across contrastive (CLIP-family) and self-supervised (DINO-family) features suggest that our UAE framework can preserve layout- and texture-level semantics that translate into more faithful reconstructions. The next tier includes BAGEL (83.48), OmniGen2 (83.31), and Janus-Pro (82.77), while BLIP-3o (76.56) and Show-o (69.16) lag notably—highlighting that strong performance in individual the understanding or generation task does not necessarily yield a higher unified score (strong mutual enhancement in the I→T→I loop.)

4.2 Text-to-Image Generation

We evaluate UAE on three benchmarks—GenEval, GenEval++, and DPG-Bench—that probe compositional understanding and instruction-following in increasingly challenging settings.

Method	Color	Count	Color/Count	Color/Pos	Pos/Count	Pos/Size	Multi-Count	Overall
Dedicated T2I								
SDv2.1 [29]	0.000	0.325	0.025	0.000	0.000	0.025	0.075	0.064
SDXL [26]	0.050	0.375	0.000	0.000	0.000	0.000	0.000	0.061
SD3-medium [1]	<u>0.550</u>	0.500	0.125	0.350	0.175	0.150	0.225	0.296
FLUX.1-Kontext [18]	0.425	0.500	0.200	0.250	<u>0.300</u>	0.400	0.325	0.343
FLUX.1-dev [18]	0.350	0.625	0.150	0.275	0.200	0.375	0.225	0.314
Unified MLLM								
Janus-Pro [5]	0.450	0.300	0.125	0.300	0.075	0.350	0.125	0.246
T2I-R1 [17]	0.675	0.325	0.200	0.350	0.075	0.250	0.300	0.311
BLIP3-o 4B [4]	0.125	0.225	0.100	0.450	0.125	<u>0.550</u>	0.225	0.257
BLIP3-o 8B [4]	0.250	0.250	0.125	0.600	0.125	0.575	0.225	0.307
OmniGen2 [36]	<u>0.550</u>	0.425	0.200	0.275	0.125	0.250	0.450	0.325
Bagel [8]	0.325	<u>0.600</u>	<u>0.250</u>	0.325	0.250	0.475	0.375	<u>0.371</u>
UAE	<u>0.550</u>	0.525	0.550	<u>0.550</u>	0.450	0.400	<u>0.400</u>	0.475

Table 3: Comparisons of instruction following generation ability on Geneval++ [13]. **Bold** indicates the best result, and underlined denotes the second best.

Method	Global	Entity	Attribute	Relation	Other	Overall
Dedicated T2I						
SDXL [26]	83.27	82.43	80.91	86.76	80.41	74.65
Hunyuan-DiT [19]	84.59	80.59	88.01	74.36	86.41	78.87
DALLE3 [22]	90.97	89.61	88.39	90.58	89.83	83.50
SD3-medium [1]	87.90	<u>91.01</u>	88.83	80.70	88.68	84.08
FLUX.1-dev [18]	82.1	89.5	88.7	<u>91.1</u>	89.4	84.0
OmniGen [37]	87.90	88.97	88.47	87.95	83.56	81.16
Unified Model						
Show-o [38]	79.33	75.44	78.02	84.45	60.80	67.27
EMU3 [33]	85.21	86.68	86.84	90.22	83.15	80.60
TokenFlow-XL [27]	78.72	79.22	81.29	85.22	71.20	73.38
Janus Pro [5]	86.90	88.90	89.40	89.32	<u>89.48</u>	84.19
BLIP3-o 4B [4]	-	-	-	-	-	79.36
BLIP3-o 8B [4]	-	-	-	-	-	81.60
UniWorld-V1 [20]	83.64	88.39	88.44	89.27	87.22	81.38
OmniGen2 [36]	88.81	88.83	90.18	89.37	90.27	83.57
BAGEL [8]	<u>88.94</u>	90.37	<u>91.29</u>	90.82	88.67	85.07
UAE	83.11	91.43	91.49	92.07	84.32	<u>84.74</u>

Table 4: Comparisons of text-to-image generation ability on DPG-Bench [16] benchmark. **Bold** indicates the best result, and underlined denotes the second best.

GenEval. As shown in Tab. 2, without considering LLM rewriting, our UAE attains the best *Overall* score among unified models (**0.86**). It leads on *Counting* (0.84) and *Color attribution* (0.79; +16 points vs. Bagel’s 0.63 and +3 vs. OmniGen2’s 0.76), co-leads on *Colors* (0.90), is second-best on *Position* (0.71), and reaches 0.89 on *Two object* (below the strongest 0.94–0.95). When considering LLM rewriting, e.g., using the same rewritten prompts with Bagel, our UAE achieves an overall score of 0.89 on average, demonstrating the SOTA performance in the image generation task.

GenEval++ (harder compositional control). GenEval++ [42] extends GenEval to prompts with *three or more* objects, each bearing distinct attributes and spatial relations, demanding comprehensive, multi-constraint satisfaction. In Tab. 3, UAE achieves the best *Overall* score (**0.475**), leading on

Method	CLIP [28]	LongCLIP [44]	DINO-v2 [24]	DINO-v3 [31]	Overall
Qwen-2.5-VL-3B [3]	88.34	92.62	73.91	70.02	80.85
Qwen-2.5-VL-7B [3]	88.26	92.89	76.12	70.96	81.92
UAE	90.50	94.35	81.98	77.54	86.09

Table 5: Comparisons of captions produced by the understanding model for better text-to-image generation. **Bold** indicates the best result, and underlined denotes the second best.

Color/Count (0.550) and *Pos/Count* (0.450), with runner-up performance on *Color/Pos* (0.550) and *Multi-Count* (0.400). Qualitative visualizations in Fig. 3 further show accurate attribute binding, disambiguation across multiple entities, and robust position–count consistency under long, constraint-heavy prompts.

DPG-Bench. On DPG-Bench (Tab. 4), UAE achieves the top scores on *Entity* (91.43), *Attribute* (91.49), and *Relation* (92.07), and ranks second overall with **84.74**, closely trailing Bagel (85.07). The sub-score pattern suggests UAE’s advantages come from faithful entity grounding and relation handling under long prompts, translating into competitive end-to-end generation quality within a unified architecture.

4.3 Improving Understanding Model as Better Captioner

Core idea and training. Fig. 1 demonstrates that *generation can benefit understanding*. We turn the generator together with a reconstruction–similarity model (our unified-score) into a **reward model** for training the understanding module as a stronger captioner. Instead of optimizing only for readability, the captioner is directly optimized for *reconstructability*: it must describe the input image comprehensively and precisely so that the generator, conditioned on this caption, can reproduce all semantics of the original image.

A better captioner for generation. Under the Unified-Bench "caption→generate→compare" protocol, captions produced by our trained understanding model yield the highest reconstruction similarity across all four backbones (Tab. 5): **90.50** (CLIP), **94.35** (LongCLIP), **81.98** (DINO-v2), **77.54** (DINO-v3), with **86.09** Overall. Relative to Qwen-2.5-VL-7B (Overall 81.92) and 3B (80.85), our gains are especially pronounced on the DINO family. These results indicate that the caption generated by our understanding model is more suitable for generation, showing the stronger preservation of object structure and fine-grained, layout-aware semantics that matter for faithful reconstruction.

Caption quality by commercial LLM judges. We further assess caption quality via pairwise comparisons against diverse opponents using four commercial LLM judges (Claude-4.1, GPT-4o, Grok-4, o4-mini). The prompt used for calling these LLMs is shown in Fig. 10. As shown in Tab. 6, our understanding model (using Qwen-2.5-VL-3B as the baseline) attains high average win rates: **94.7** vs. Show-o, **71.4** vs. OmniGen2, **64.3** vs. Bagel, and **76.3/71.5** vs. Qwen-2.5-VL (3B/7B), while remaining competitive with GPT-4o (47.2). The cross-judge agreement suggests our captions improve along multiple axes—completeness, attribute binding, relational and spatial fidelity—precisely the properties rewarded by the reconstruction-driven training signal.

4.4 Qualitative Analysis

GenEval++ visualizations. Fig. 5 presents six representative prompts from GenEval++ [42], where each instruction contains *three or more* entities with distinct attributes and spatial relations. Across these examples, UAE shows three recurring strengths. First, it preserves *attribute binding* under multi-entity scenes: for “three *purple* hair dryers and one *pink* surfboard,” UAE attaches colors to the correct categories without leakage, whereas baselines often color a surfboard purple or mix pink/purple across objects. Second, UAE is more reliable on *discrete counts* while respecting co-occurring constraints: for “three beds on the above and three parking meters on the below,” UAE maintains the 3+3 cardinality *and* the vertical arrangement; competing models tend to be off-by-one or satisfy the layout but drop a meter/bed. Third, UAE handles *left/right and grouping* more faithfully: for “an *orange* laptop on the *left* and a *purple* knife on the *right*,” our outputs keep the polarity and

Opponent	# Param	Claude-4.1	GPT-4o	Grok-4	o4-mini	Avg
GPT-4o [23]	-	47.4	89.4	30.6	21.2	47.2
Bagel [8]	7B	57.7	92.9	58.3	48.2	64.3
OmniGen2 [36]	3B	67.9	97.6	63.5	56.5	71.4
Show-o [38]	1.3B	97.8	100.0	89.8	91.0	94.7
Qwen-2.5-VL-3B [3]	3B	76.3	99.0	67.0	63.0	76.3
Qwen-2.5-VL-7B [3]	7B	68.8	99.0	62.0	56.0	71.5

Table 6: **Pairwise winning rate (%)** of our trained understanding model (3B) against different opponents on Unified-Bench, evaluated by four judge models (using official commercial API). The **Avg** column reports the mean score across judges.

avoid color–object swaps that are common failure modes. Similar advantages emerge in the “two cows, two books, and one donut” and “six vases” prompts: UAE balances global composition with local details, maintaining counts while rendering plausible object geometry and material. These observations align with Tab. 3: UAE leads on *Color/Count* and *Pos/Count*, and is competitive on *Color/Pos* and *Multi-Count*, reflecting robust satisfaction of *joint* constraints rather than excelling on a single dimension.

An “aha moment” in Multimodal from RL. Fig. 1 and Fig. 6 illustrate how reinforcement learning with a *generator + reconstruction-similarity* reward tightens the understanding–generation loop. Visually, as training proceeds from left to right, captions produced by the understanding model become more *complete and specific*: early captions tend to state category and a few salient attributes; mid-training captions begin to enumerate counts, colors, and spatial relations; later captions systematically cover accessories, materials, occlusions, backgrounds, and lighting (e.g., “yellow knitted beanie,” “navy blue knitted turtleneck sweater,” “black-framed glasses,” “ears are not visible,” “blurred background, park-like setting”). In lockstep, reconstructions grow closer to the source image. The bottom trend lines show two correlated signals: caption length increases (a proxy for semantic coverage) and the unified reward rises, with noticeable jumps whenever the captioner starts capturing previously omitted constraints (e.g., adding left/right or exact cardinalities). While longer captions are not inherently better, here the *content* added through RL is the kind that most directly benefits reconstruction, which is precisely what the reward encourages.

Unified-Bench case study. Fig. 7 contrasts captions used for reconstruction on a challenging example (small black dog wearing a yellow beanie and glasses). Baselines reveal three typical errors. (i) *Category drift*: some misidentify the subject as a monkey, causing the generator to synthesize an incorrect species. (ii) *Attribute omissions or swaps*: descriptions drop key items (beanie, glasses) or mismatch apparel colors, leading to reconstructions that caricature the outfit. (iii) *Under-specified scenes*: vague backgrounds and missing lighting cues prevent consistent photographic style at inference. UAE’s caption, in contrast, enumerates the full set of semantics—species, apparel *type and color*, eyewear, pose, occlusions (“ears are not visible”), background style (“blurred, park-like”), and lighting—producing a reconstruction that preserves identity, attire, and overall aesthetic. This example typifies the mechanism by which better understanding (denser, better-bound descriptions) yields better generation, echoing our Unified-Bench gains in Tab. 5.

5 Discussion

On image-to-image (I2I) reconstruction. In Stage-3 (Fig. 2), we explore an *alternative branch* that replaces the long-caption embedding with a dense *image* embedding from the visual encoder (similar to [32]). Although an image embedding is, in principle, richer than text, our experiments show that after long-text RL in Stage-3, subsequent I2I RL brings only marginal gains. We therefore view the two routes—long, highly descriptive captions vs. image embeddings—as *near-equivalent* in practice: both are produced in the same output space (Qwen’s conditioning embedding) and carry comparable semantic information for reconstruction. In short, once a model has been trained to produce sufficiently descriptive long text, switching to I2I reconstruction could deliver little additional benefit, suggesting functional equivalence between the two Stage-3 “alternatives”.

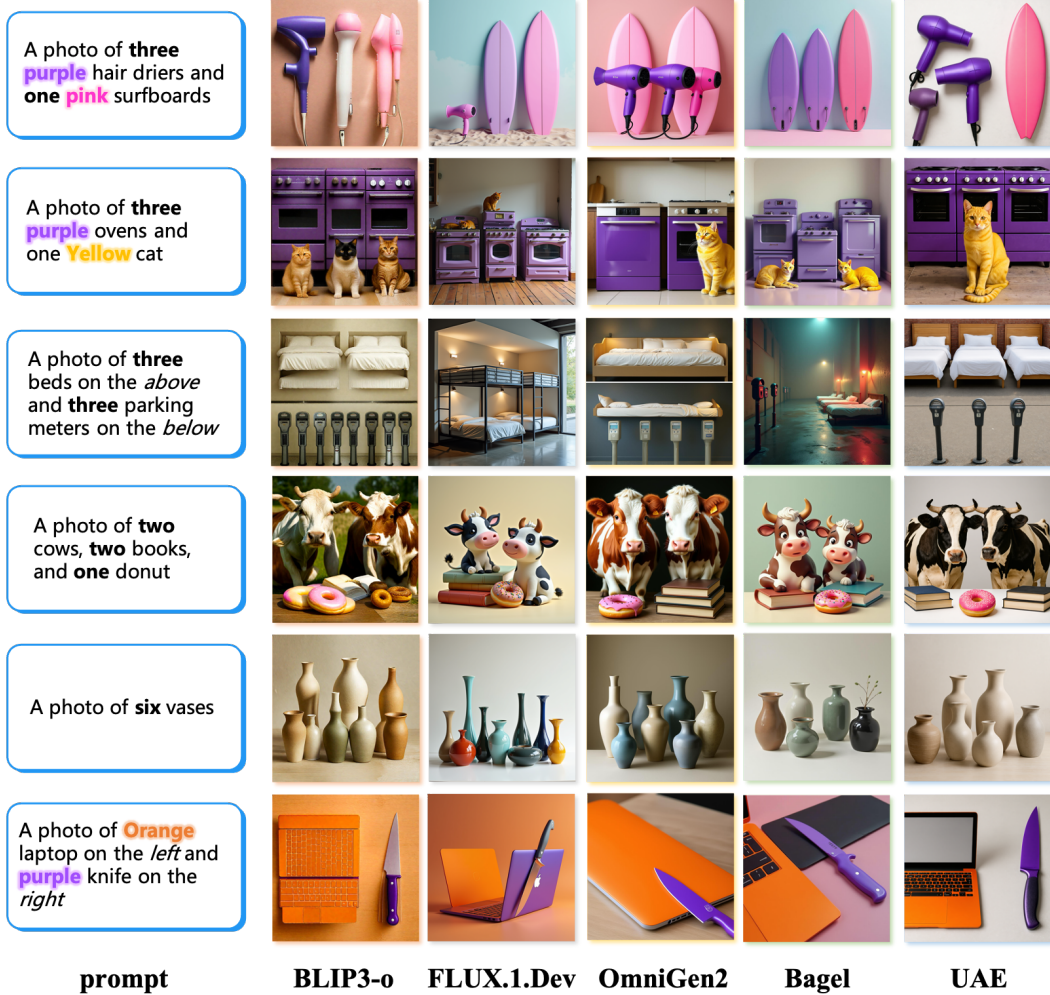


Figure 5: Qualitative analysis of the results from GenEval++, where our UAE demonstrates visually consistent results aligned with the input captions, and performs reasonable composition for each element.

On image editing. We regard editing as a natural extension of I2I reconstruction with an added requirement: *pixel-level* preservation outside edited regions. Operationally, editing still ingests an image (plus a brief instruction), obtains an output embedding via the LVLN, and renders with the generator; however, the objective differs—beyond semantic fidelity, one must minimize deviation (e.g., MSE) on untouched pixels. This favors injecting *VAE image embeddings* that encode low-level texture, geometry, and lighting, which recent strong editors (e.g., Qwen-Image [34], ImgEdit-E1 [43]) explicitly exploit. By contrast, systems that appear to rely primarily on semantic conditioning (e.g., without explicit VAE latents) tend to reconstruct global semantics yet struggle to perfectly preserve non-edited regions. Extending UAE to editing is therefore a straightforward conceptually: augment the conditioning with VAE latents and train with a reconstruction objective that jointly optimizes semantic compliance and pixel preservation within a masked loss.

On text rendering. Text rendering is a current limitation. Our training data contains a few high-quality, text-rich image-caption pairs at ≥ 1024 resolution, and we did not perform targeted text-specific RL. Prior work (e.g., X-Omni [12]) shows that OCR-based rewards during RL substantially improve typography fidelity; recent results (e.g., Qwen-Image [34]) further underscore the importance of such supervision. Because our goal here is to present a *unified objective and training paradigm* rather than a feature-complete product, we focus RL on reconstruction similarity rather than OCR rewards. A natural next step is **Unified-GRPO for text**, where the understanding module must

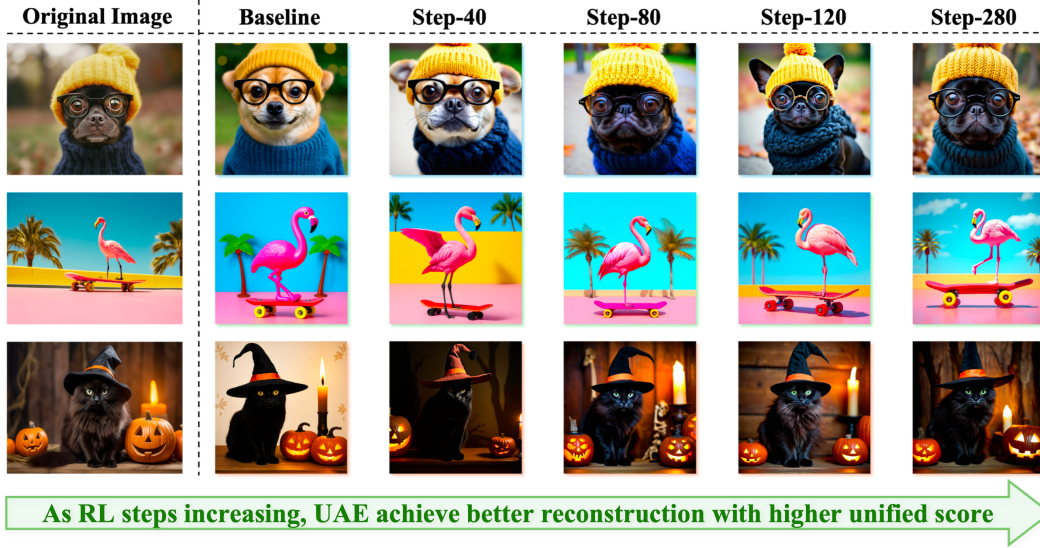


Figure 6: Illustration of the generated results via our unified-GRPO, with the RL steps increasing, the understanding model (encoder) achieves better caption capability to produce a longer, detailed, yet accurate caption to reconstruct the original image comprehensively; while the generation model (decoder) can take the detailed caption as input for better generation.

capture glyph content and layout, and the generator is rewarded for reconstructing the original text. This finer-grained objective is likely to strengthen both understanding and generation in scenes containing signs, documents, and UI elements.

On architectural evolution. In the first version of this work, we intentionally adopt a minimal encoder–connector–decoder design (in the spirit of UniWorld-V1 [20]) to present the auto-encoder perspective as transparently as possible. Looking ahead, we plan two upgrades. First, refine the *connector* to better align the LVLM’s output space with the diffusion decoder’s conditioning space (e.g., structured adapters, multi-scale cross-attention, or loss-aware projection). Second, push the diffusion component toward a *pure decoder* and further *decouple* understanding and generation: the encoder focuses solely on semantic compression ($I \rightarrow T$ or $I \rightarrow E$), the decoder on semantic decompression ($T/E \rightarrow I$), and unification arises from a single reconstruction objective that drives mutual benefit. This tighter adherence to the auto-encoder principle should yield cleaner interfaces, more stable RL, and clearer pathways for plugging in specialized capabilities (e.g., editing via VAE latents, OCR-aware text rendering) without entangling the two halves of the system.

On long-text supervision and conditioning. We argue that **long text** is foundational across *all* tasks—understanding, generation, I2I, and editing—because it provides a higher-bandwidth alignment signal between vision and language [2]. From an alignment perspective, longer captions encode more complete semantics (entities, attributes, relations, counts, occlusions, background, lighting, style), reducing ambiguity in the conditioning and tightening the $I \leftrightarrow T$ mapping. For *understanding*, a captioner trained to produce *very detailed* descriptions must extract and organize nearly all recoverable image evidence; this improves coverage and attribute binding, and—under our unified reward—directly optimizes for reconstructability rather than mere fluency. For *generation*, a decoder that can consume very long prompts can, in principle, render every clause of a sufficiently descriptive caption (e.g., turning “draw a tangyuan” into “a Chinese dessert... white, glutinous exterior with black sesame filling. ...”), thereby collapsing instruction ambiguity and improving semantic fidelity. The same logic extends to *I2I*: a dense visual embedding can be viewed as an extreme case of a “very long” textual embedding that covers the entire scene; empirically, once Stage-3 long-text RL is in place, further I2I RL yields limited gains, supporting the practical near-equivalence between long-text conditioning and image-embedding conditioning in our framework. For *editing*, long text specifies what to change and what to preserve; combined with VAE latents for low-level pixel retention, long prompts help constrain edits to semantically precise, spatially localized operations.

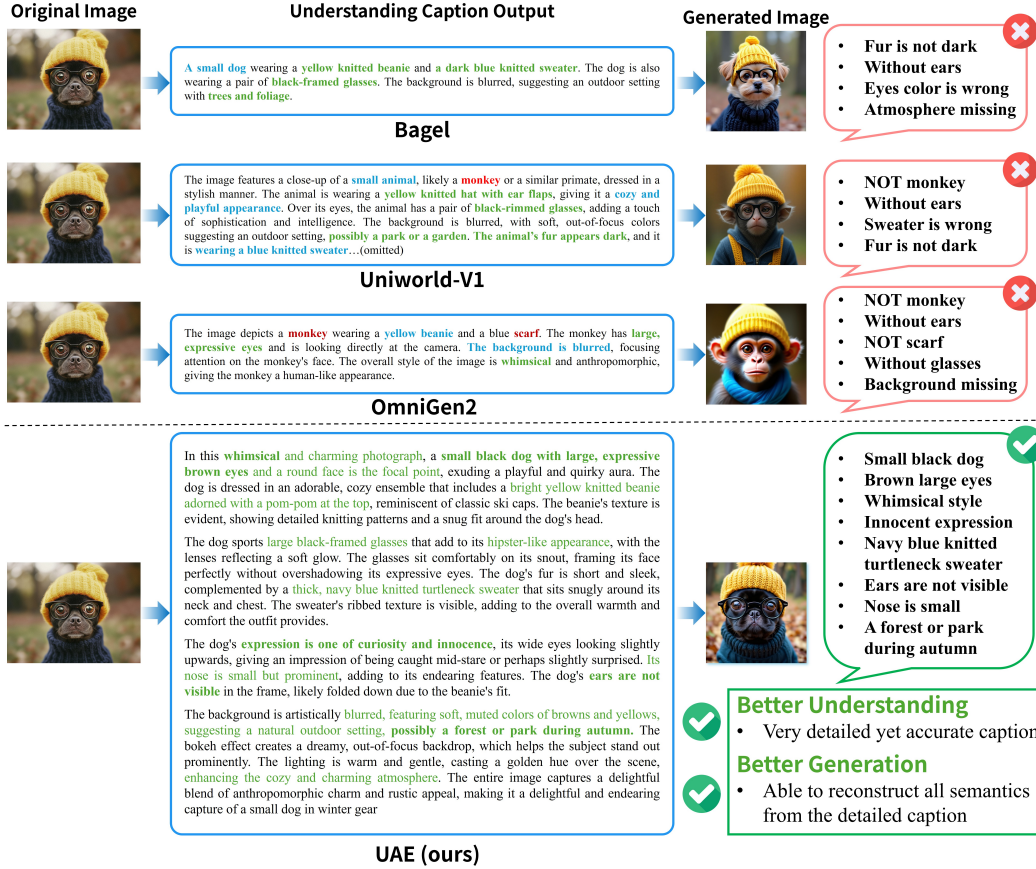


Figure 7: Case study of the results from the proposed Unified-Bench, we see that our UAE enables to produce a more detailed, accurate, comprehensive description based on the input image, and reconstructs a similar result to the original image, showcasing the improved understanding and generation capabilities, and the better unification of the system.

We also observe that GPT-4o-Image accepts *very long* inputs and reproduces their semantics with high fidelity, suggesting it has likely been fine-tuned on long-text supervision to internalize such granular constraints. However, despite its importance, the community still lacks a truly large-scale, high-resolution long-text corpus. This motivates our curated 700K long-text image-caption set (above 250 English words, 1024-px images): it supplies the missing bandwidth for training captioners that cover *all* salient details and generators that can condition on them. Practically, long-text training introduces computational and modeling challenges (context length, positional extrapolation, redundancy control). Our design addresses these via a lightweight projector/connector, reconstruction-based rewards that favor *salient* details over verbosity, and RL signals that penalize omissions and contradictions—turning long text from a liability into a precise, high-information interface that consistently improves unified performance.

6 Conclusion

We show that an auto-encoder is a viable core for unifying multimodal understanding and generation. Building on this idea, we introduce UAE, which warms up the decoder on long-context captions. We then propose Unified-GRPO, a three-stage RL procedure—cold-start-reconstruction, Generation-for-Understanding and Understanding-for-Generation—that jointly optimizes caption informativeness and reconstruction fidelity. To quantify progress toward unification, we present Unified-Bench, the first evaluation tailored to the bidirectional nature of UMMs. During training, we observe an "aha moment": captions become longer and more precise while reconstructions sharpen, evidencing coherent, bidirectional information flow. Together, these components offer a clear recipe and measurement protocol for building truly unified multimodal models.

References

- [1] Stability AI. Sd3-medium. <https://stability.ai/news/stable-diffusion-3-medium>, 2024.
- [2] Hyojin Bahng, Caroline Chan, Fredo Durand, and Phillip Isola. Cycle consistency as reward: Learning image-text alignment without human preferences. *arXiv preprint arXiv:2506.02095*, 2025.
- [3] Shuai Bai, Keqin Chen, Xuejing Liu, Jialin Wang, Wenbin Ge, Sibao Song, Kai Dang, Peng Wang, Shijie Wang, Jun Tang, et al. Qwen2. 5-vl technical report. *arXiv preprint arXiv:2502.13923*, 2025.
- [4] Jiu hai Chen, Zhiyang Xu, Xichen Pan, Yushi Hu, Can Qin, Tom Goldstein, Lifu Huang, Tianyi Zhou, Saining Xie, Silvio Savarese, et al. Blip3-o: A family of fully open unified multimodal models-architecture, training and dataset. *arXiv preprint arXiv:2505.09568*, 2025.
- [5] Xiaokang Chen, Zhiyu Wu, Xingchao Liu, Zizheng Pan, Wen Liu, Zhenda Xie, Xingkai Yu, and Chong Ruan. Janus-pro: Unified multimodal understanding and generation with data and model scaling. *arXiv preprint arXiv:2501.17811*, 2025.
- [6] Zhe Chen, Jiannan Wu, Wenhai Wang, Weijie Su, Guo Chen, Sen Xing, Muyan Zhong, Qinglong Zhang, Xizhou Zhu, Lewei Lu, et al. Internvl: Scaling up vision foundation models and aligning for generic visual-linguistic tasks. In *Proceedings of the IEEE/CVF Conference on Computer Vision and Pattern Recognition*, pp. 24185–24198, 2024.
- [7] DeepFloyd. Github link: <https://github.com/deep-floyd/if>, 2023. URL <https://github.com/deep-floyd/IF>.
- [8] Chaorui Deng, Deyao Zhu, Kunchang Li, Chenhui Gou, Feng Li, Zeyu Wang, Shu Zhong, Weihao Yu, Xiaonan Nie, Ziang Song, et al. Emerging properties in unified multimodal pretraining. *arXiv preprint arXiv:2505.14683*, 2025.
- [9] Haoge Deng, Ting Pan, Haiwen Diao, Zhengxiong Luo, Yufeng Cui, Huchuan Lu, Shiguang Shan, Yonggang Qi, and Xinlong Wang. Autoregressive video generation without vector quantization. *arXiv preprint arXiv:2412.14169*, 2024.
- [10] Patrick Esser, Sumith Kulal, Andreas Blattmann, Rahim Entezari, Jonas Müller, Harry Saini, Yam Levi, Dominik Lorenz, Axel Sauer, Frederic Boesel, et al. Scaling rectified flow transformers for high-resolution image synthesis. In *Forty-first International Conference on Machine Learning*, 2024.
- [11] Yuying Ge, Sijie Zhao, Jinguo Zhu, Yixiao Ge, Kun Yi, Lin Song, Chen Li, Xiaohan Ding, and Ying Shan. Seed-x: Multimodal models with unified multi-granularity comprehension and generation, 2024. URL <https://arxiv.org/abs/2404.14396>.
- [12] Zigang Geng, Yibing Wang, Yeyao Ma, Chen Li, Yongming Rao, Shuyang Gu, Zhao Zhong, Qinglin Lu, Han Hu, Xiaosong Zhang, et al. X-omni: Reinforcement learning makes discrete autoregressive image generative models great again. *arXiv preprint arXiv:2507.22058*, 2025.
- [13] Dhruva Ghosh, Hannaneh Hajishirzi, and Ludwig Schmidt. Geneval: An object-focused framework for evaluating text-to-image alignment. *Advances in Neural Information Processing Systems*, 36, 2024.
- [14] Agrim Gupta, Linxi Fan, Surya Ganguli, and Li Fei-Fei. Metamorph: Learning universal controllers with transformers. *arXiv preprint arXiv:2203.11931*, 2022.
- [15] Edward J Hu, Yelong Shen, Phillip Wallis, Zeyuan Allen-Zhu, Yuanzhi Li, Shean Wang, Lu Wang, Weizhu Chen, et al. Lora: Low-rank adaptation of large language models. *ICLR*, 1(2):3, 2022.
- [16] Xiwei Hu, Rui Wang, Yixiao Fang, Bin Fu, Pei Cheng, and Gang Yu. Ella: Equip diffusion models with llm for enhanced semantic alignment. *arXiv preprint arXiv:2403.05135*, 2024.
- [17] Dongzhi Jiang, Ziyu Guo, Renrui Zhang, Zhuofan Zong, Hao Li, Le Zhuo, Shilin Yan, Pheng-Ann Heng, and Hongsheng Li. T2i-r1: Reinforcing image generation with collaborative semantic-level and token-level cot. *arXiv preprint arXiv:2505.00703*, 2025.
- [18] Black Forest Labs. Flux. <https://github.com/black-forest-labs/flux>, 2024.
- [19] Zhimin Li, Jianwei Zhang, Qin Lin, Jiangfeng Xiong, Yanxin Long, Xincheng Deng, Yingfang Zhang, Xingchao Liu, Minbin Huang, Zedong Xiao, et al. Hunyuan-dit: A powerful multi-resolution diffusion transformer with fine-grained chinese understanding. *arXiv preprint arXiv:2405.08748*, 2024.

- [20] Bin Lin, Zongjian Li, Xinhua Cheng, Yuwei Niu, Yang Ye, Xianyi He, Shenghai Yuan, Wangbo Yu, Shaodong Wang, Yunyang Ge, et al. Uniworld: High-resolution semantic encoders for unified visual understanding and generation. *arXiv preprint arXiv:2506.03147*, 2025.
- [21] Jie Liu, Gongye Liu, Jiajun Liang, Yangguang Li, Jiaheng Liu, Xintao Wang, Pengfei Wan, Di Zhang, and Wanli Ouyang. Flow-grpo: Training flow matching models via online rl. *arXiv preprint arXiv:2505.05470*, 2025.
- [22] OpenAI. Dall-e 3. <https://openai.com/index/dall-e-3>, 2024.
- [23] OpenAI. Gpt-4o. <https://openai.com/index/introducing-4o-image-generation>, 2025.
- [24] Maxime Oquab, Timothée Darcet, Théo Moutakanni, Huy Vo, Marc Szafraniec, Vasil Khalidov, Pierre Fernandez, Daniel Haziza, Francisco Massa, Alaaeldin El-Nouby, et al. Dinov2: Learning robust visual features without supervision. *arXiv preprint arXiv:2304.07193*, 2023.
- [25] Xichen Pan, Satya Narayan Shukla, Aashu Singh, Zhuokai Zhao, Shlok Kumar Mishra, Jialiang Wang, Zhiyang Xu, Jiuhai Chen, Kunpeng Li, Felix Juefei-Xu, et al. Transfer between modalities with metaqueries. *arXiv preprint arXiv:2504.06256*, 2025.
- [26] Dustin Podell, Zion English, Kyle Lacey, Andreas Blattmann, Tim Dockhorn, Jonas Müller, Joe Penna, and Robin Rombach. Sdxl: Improving latent diffusion models for high-resolution image synthesis. *arXiv preprint arXiv:2307.01952*, 2023.
- [27] Liao Qu, Huichao Zhang, Yiheng Liu, Xu Wang, Yi Jiang, Yiming Gao, Hu Ye, Daniel K Du, Zehuan Yuan, and Xinglong Wu. Tokenflow: Unified image tokenizer for multimodal understanding and generation. In *Proceedings of the Computer Vision and Pattern Recognition Conference*, pp. 2545–2555, 2025.
- [28] Alec Radford, Jong Wook Kim, Chris Hallacy, Aditya Ramesh, Gabriel Goh, Sandhini Agarwal, Girish Sastry, Amanda Askell, Pamela Mishkin, Jack Clark, et al. Learning transferable visual models from natural language supervision. In *International conference on machine learning*, pp. 8748–8763. PmLR, 2021.
- [29] Robin Rombach, Andreas Blattmann, Dominik Lorenz, Patrick Esser, and Björn Ommer. High-resolution image synthesis with latent diffusion models. In *Proceedings of the IEEE/CVF conference on computer vision and pattern recognition*, pp. 10684–10695, 2022.
- [30] Zhihong Shao, Peiyi Wang, Qihao Zhu, Runxin Xu, Junxiao Song, Xiao Bi, Haowei Zhang, Mingchuan Zhang, YK Li, Yang Wu, et al. Deepseekmath: Pushing the limits of mathematical reasoning in open language models. *arXiv preprint arXiv:2402.03300*, 2024.
- [31] Oriane Siméoni, Huy V Vo, Maximilian Seitzer, Federico Baldassarre, Maxime Oquab, Cijo Jose, Vasil Khalidov, Marc Szafraniec, Seungeun Yi, Michaël Ramamonjisoa, et al. Dinov3. *arXiv preprint arXiv:2508.10104*, 2025.
- [32] Haochen Wang, Anlin Zheng, Yucheng Zhao, Tiancai Wang, Zheng Ge, Xiangyu Zhang, and Zhaoxiang Zhang. Reconstructive visual instruction tuning. *arXiv preprint arXiv:2410.09575*, 2024.
- [33] Xinlong Wang, Xiaosong Zhang, Zhengxiong Luo, Quan Sun, Yufeng Cui, Jinsheng Wang, Fan Zhang, Yueze Wang, Zhen Li, Qiying Yu, et al. Emu3: Next-token prediction is all you need. *arXiv preprint arXiv:2409.18869*, 2024.
- [34] Chenfei Wu, Jiahao Li, Jingren Zhou, Junyang Lin, Kaiyuan Gao, Kun Yan, Sheng-ming Yin, Shuai Bai, Xiao Xu, Yilei Chen, et al. Qwen-image technical report. *arXiv preprint arXiv:2508.02324*, 2025.
- [35] Chengyue Wu, Xiaokang Chen, Zhiyu Wu, Yiyang Ma, Xingchao Liu, Zizheng Pan, Wen Liu, Zhenda Xie, Xingkai Yu, Chong Ruan, et al. Janus: Decoupling visual encoding for unified multimodal understanding and generation. In *Proceedings of the Computer Vision and Pattern Recognition Conference*, pp. 12966–12977, 2025.
- [36] Chenyuan Wu, Pengfei Zheng, Ruirao Yan, Shitao Xiao, Xin Luo, Yueze Wang, Wanli Li, Xiyan Jiang, Yexin Liu, Junjie Zhou, et al. Omnigen2: Exploration to advanced multimodal generation. *arXiv preprint arXiv:2506.18871*, 2025.
- [37] Shitao Xiao, Yueze Wang, Junjie Zhou, Huaying Yuan, Xingrun Xing, Ruirao Yan, Chaofan Li, Shutong Wang, Tiejun Huang, and Zheng Liu. Omnigen: Unified image generation. In *Proceedings of the Computer Vision and Pattern Recognition Conference*, pp. 13294–13304, 2025.

- [38] Jinheng Xie, Weijia Mao, Zechen Bai, David Junhao Zhang, Weihao Wang, Kevin Qinghong Lin, Yuchao Gu, Zhijie Chen, Zhenheng Yang, and Mike Zheng Shou. Show-o: One single transformer to unify multimodal understanding and generation. *arXiv preprint arXiv:2408.12528*, 2024.
- [39] Jinheng Xie, Weijia Mao, Zechen Bai, David Junhao Zhang, Weihao Wang, Kevin Qinghong Lin, Yuchao Gu, Zhijie Chen, Zhenheng Yang, and Mike Zheng Shou. Show-o: One Single Transformer to Unify Multimodal Understanding and Generation, October 2024.
- [40] Zhiyuan Yan, Jiangming Wang, Zhendong Wang, Peng Jin, Ke-Yue Zhang, Shen Chen, Taiping Yao, Shouhong Ding, Baoyuan Wu, and Li Yuan. Effort: Efficient orthogonal modeling for generalizable ai-generated image detection. *arXiv preprint arXiv:2411.15633*, 2, 2024.
- [41] Zhiyuan Yan, Junyan Ye, Weijia Li, Zilong Huang, Shenghai Yuan, Xiangyang He, Kaiqing Lin, Jun He, Conghui He, and Li Yuan. Gpt-imgeval: A comprehensive benchmark for diagnosing gpt4o in image generation. *arXiv preprint arXiv:2504.02782*, 2025.
- [42] Junyan Ye, Dongzhi Jiang, Zihao Wang, Leqi Zhu, Zhenghao Hu, Zilong Huang, Jun He, Zhiyuan Yan, Jinghua Yu, Hongsheng Li, et al. Echo-4o: Harnessing the power of gpt-4o synthetic images for improved image generation. *arXiv preprint arXiv:2508.09987*, 2025.
- [43] Yang Ye, Xianyi He, Zongjian Li, Bin Lin, Shenghai Yuan, Zhiyuan Yan, Bohan Hou, and Li Yuan. Imgedit: A unified image editing dataset and benchmark. *arXiv preprint arXiv:2505.20275*, 2025.
- [44] Beichen Zhang, Pan Zhang, Xiaoyi Dong, Yuhang Zang, and Jiaqi Wang. Long-clip: Unlocking the long-text capability of clip. In *European conference on computer vision*, pp. 310–325. Springer, 2024.
- [45] Chunting Zhou, Lili Yu, Arun Babu, Kushal Tirumala, Michihiro Yasunaga, Leonid Shamis, Jacob Kahn, Xuezhe Ma, Luke Zettlemoyer, and Omer Levy. Transfusion: Predict the next token and diffuse images with one multi-modal model. *arXiv preprint arXiv:2408.11039*, 2024.
- [46] Le Zhuo, Ruoyi Du, Han Xiao, Yangguang Li, Dongyang Liu, Rongjie Huang, Wenze Liu, Xiangyang Zhu, Fu-Yun Wang, Zhanyu Ma, et al. Lumina-next: Making lumina-t2x stronger and faster with next-dit. *Advances in Neural Information Processing Systems*, 37:131278–131315, 2024.



This is an image showcasing traditional Chinese dim sum, with a warm color palette dominated by bamboo steamers and a dark background, creating a rustic and homely atmosphere.

Overall Composition and Angle

- **Photography Angle:** Top-down with a slight tilt, allowing clear visibility of the details and placement of each dim sum.
- **Background Material:** A dark, rough tabletop paired with a light bamboo steamer, giving a warm and rustic tone.
- **Composition:** The steamer is at the center with four dim sum pieces. Two small bowls of tea are placed in the upper left corners, creating a symmetrical and balanced visual.

Main Food Components

1. Dim Sum (Center)

- **Quantity and Position:** Four translucent dumplings in a diamond shape, evenly placed in the steamer with appropriate spacing.
- **Shape and Color:** The dumplings have a transparent outer skin, diamond-shaped, with colorful fillings including green vegetables, orange carrots, and white meat.
- **Material and Details:** The skin is thin and transparent, clearly showing the filling inside, with a smooth and slightly glossy surface.

2. Tea Bowls (Upper Left Corners)

- **Quantity and Position:** Two small tea bowls located in the upper left and lower left corners.
- **Shape and Color:** The bowls are round with a dark brown exterior and white interior, filled with clear, orange-red tea.
- **Material and Details:** The bowls are ceramic with a smooth surface, and the tea has a rich color, indicating its aroma and texture.

Background and Environment

- **Background Material:** A dark, rough tabletop that contrasts sharply with the bamboo steamer, highlighting the dim sum.
- **Steamer Details:** Bamboo steamer with a partially open lid revealing the dim sum inside. The bottom of the steamer is lined with white baking paper, marked with bamboo patterns.

Artistic Style and Techniques

- **Style:** Realistic, focusing on detail and texture representation.
- **Lighting Effects:** Soft, even lighting on the dim sum and tea bowls, emphasizing texture and color without harsh shadows.
- **Perspective and Angle:** Top-down view, making the composition clear and allowing full visibility of details.

Language Standards

- **Objective Description:** Only visible content is described, without speculation or unrelated information.

Conciseness

- **Precise Description:** Core information is covered concisely, avoiding redundancy. To accurately recreate this image, ensure the following elements:
 - A central bamboo steamer with four translucent diamond-shaped dumplings with colorful fillings.
 - Two small tea bowls with dark brown exteriors and white interiors, containing orange-red tea, placed in the upper left corners.
 - A dark, rough tabletop background contrasting with the bamboo steamer to highlight the dim sum.
 - Soft, even lighting to emphasize the texture and color of the food.

Figure 8: Visual example of the proposed 700K long-context text-to-image dataset.



This is an indoor photograph depicting a man engaged in traditional grain processing, creating a warm and historically rich atmosphere.

General Overview

In the photo, a man is winnowing grain with a tray, set against a dimly lit indoor background with soft lighting, evoking an ancient and focused ambiance.

Main Subject Identification

- **Core Subject:** A man positioned slightly to the right of the center.
- **Ethnicity and Age:** The man appears to be of Asian descent, aged between 30 and 40.
- **Expression:** His expression is concentrated, with his gaze fixed on the grain in the tray.

Detail Characteristics

- **Attire:** The man is wearing a dark jacket over a red garment, with a circular badge on the jacket.
- **Hair:** Short and neatly styled.
- **Tray:** He holds a light-colored bamboo tray with both hands, which is semi-circular and made of natural bamboo.
- **Grain:** The grain in the tray is light yellow, being tossed to form an arc towards the ground.

Quantity and Position

- **Number of Subjects:** One person.
- **Position:** The man is slightly to the right of the center, with the tray between his hands, and grain being scattered onto a pile on the ground.
- **Background:** There are several large grain piles in the background, dome-shaped, located behind and to the left of the man.

Actions and Background

- **Action:** The man holds the tray with both hands, slightly leaning forward, with his right hand on the right side of the tray and his left on the left, winnowing the grain. His legs are slightly apart for balance.
- **Background Scene:** The setting is a wooden indoor structure with dim lighting. A bright bulb hangs from the ceiling, casting a warm yellow glow. The air is filled with grain dust, adding dynamism to the scene.

Artistic Style and Techniques

- **Style:** Realistic, emphasizing detail and texture.
- **Lighting Effects:** Light from above creates a Tyndall effect, making the grain dust visible and enhancing the depth of the image.
- **Framing and Perspective:** Medium shot, centered composition, with the camera angle slightly below the man's eye level, making the subject more prominent and lifelike.

Language Standards

- **Objective Description:** Only visible content is described, without speculation or irrelevant information.

Conciseness

- **Precise Description:** Covers all core information, avoiding redundancy. This detailed description comprehensively captures the scene and atmosphere of the photograph.

Figure 9: Visual example of the proposed 700K long-context text-to-image dataset.

```

"""
You are an expert in language analysis and computer vision. Your task is to act as an impartial judge and evaluate two
captions, generated by Model A and Model B, for the provided source image. Your evaluation must be exceptionally detailed
and comprehensive.

You will conduct a multi-dimensional analysis of each caption based on the specific criteria listed below. For each criterion,
you will assign a score from 1 (very poor) to 10 (excellent). After scoring, you must provide a detailed, structured
comparative analysis and declare a final winner.

**Evaluation Criteria & Scoring:**

Please evaluate each caption against the following four criteria. Provide your scores in a markdown table.

1. **Comprehensiveness, Descriptive Richness, and Accuracy:**
    * How deeply does the caption describe the image? Does it go beyond a superficial glance to include important, specific
      details (e.g., colors, textures, materials, lighting, background elements, expressions)?
    * Does it effectively and accurately describe the context (e.g., a black dog not a monkey, or brown eyes not black),
      environment (background description)?
    * Does the caption capture subtle nuances that a casual observer might miss?

2. **Linguistic Fluency and Naturalness:**
    * Is the caption grammatically correct and well-written in natural-sounding English?
    * Does it flow like a human would describe the scene, or does it sound robotic, disjointed, or like a list of keywords?
    * Is the vocabulary choice sophisticated, appropriate, and engaging?

3. **Semantic and Compositional Insight:**
    * Does it effectively capture and convey the overall mood, atmosphere, emotion, or narrative implied by the scene?
    * Does it demonstrate an understanding of the image's composition (e.g., what is in the foreground vs. background)?

---

**Required Output Format:**

Your entire response must strictly follow this structure:

**1. Scoring Table:**
A markdown table with the scores for each criterion.

| Criterion | Caption A Score | Caption B Score |
| :--- | :---: | :---: |
| Comprehensiveness, Descriptive Richness, and Accuracy | [score] | [score] |
| Linguistic Fluency and Naturalness | [score] | [score] |
| Semantic and Compositional Insight | [score] | [score] |
| **Total Score** | **[sum]** | **[sum]** |

**2. Detailed Comparative Analysis:**
Provide a comprehensive, head-to-head comparison of the two captions. Structure your analysis with subheadings for each
of the four criteria. For each criterion, explicitly quote phrases from both Caption A and Caption B to illustrate your points and
justify the difference in their scores. Explain not just *what* is different, but *why* one caption's approach is superior for
describing the provided image.

**3. Final Verdict:**
Based on your total scores and detailed comparative analysis, declare the winner. This section must contain only a single
letter.

**Final Answer:** [A or B] (You should output the answer within <answer></answer>)\n
"""

img_des = """
**Source Image:**\n
"""

caption_ = """\n
**Captions to Evaluate as Generation Prompts:**
---

* **Caption A:** {}

---

* **Caption B:** {}

```

Figure 10: Original Prompt for official LLMs to judge the two captions outputted by the understanding models.